JACS
JOURNAL OF THE AMERICAN CHEMICAL SOCIETY
Article
pubs.acs.org/JACS

# Half-Metallicity in $MnPSe_3$ Exfoliated Nanosheet with Carrier Doping

Xingxing Li,[†] Xiaojun Wu,[†,‡,§] and Jinlong Yang*[,†,§]

[†]Hefei National Laboratory for Physical Science at the Microscale, University of Science and Technology of China, Hefei, Anhui 230026, China

[‡]CAS Key Laboratory of Materials for Energy Conversion and Department of Materials Science and Engineering, University of Science and Technology of China, Hefei, Anhui 230026, China

[§]Synergetic Innovation Center of Quantum Information & Quantum Physics, University of Science and Technology of China, Hefei, Anhui 230026, China

**ABSTRACT:** Searching two-dimensional (2D) half-metallic crystals that are feasible in experiment is essential to develop next-generation nanospintronic devices. Here, a 2D exfoliated $MnPSe_3$ nanosheet with novel magnetism is first proposed based on first-principles calculations. In particular, the evaluated low cleavage energy and high in-plane stiffness indicate that the free-standing $MnPSe_3$ nanosheet can be exfoliated from its bulk structure in experiment. The $MnPSe_3$ nanosheet is an antiferromagnetic semiconductor at its ground state, whereas both electron and hole doping induce its transition from antiferromagnetic semiconductor to ferromagnetic half-metal. Moreover, the spin-polarization directions of 2D half-metallic $MnPSe_3$ are opposite for electron and hole doping, which can be controlled by applying an external voltage gate. The Monte Carlo simulation based on the Ising model suggests the Curie temperature of the doped 2D $MnPSe_3$ crystal is up to 206 K. These advantages render the 2D $MnPSe_3$ crystal with great potentials for application in electric-field controlled spintronic devices.

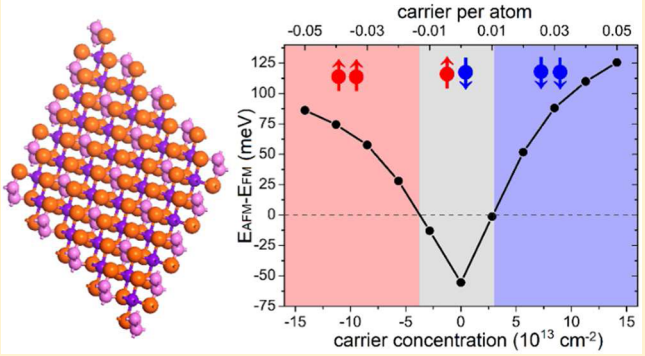


## INTRODUCTION

Spintronics, which uses the spin of electrons for information storage, transportation and processing, has attracted intensive interests from both science and industry in the past decades.[1] Half-metals with one conducting spin channel and one insulating spin channel have been considered as the ideal materials for spintronic applications.[2,3] To fabricate spintronic device at nanoscale, it is one key issue to develop low-dimensional materials with half-metallicity. Theoretically, numbers of low-dimensional half-metals have been proposed.[4−8] However, until now the experimental validation of half-metallicity in these systems has been scarce partly due to the low yield, small domains and rich boundaries/defects of prepared samples, or the difficulty in obtaining crystalline structures.[9−11] Searching experimentally feasible low-dimensional half-metals still remains a big challenge.

Another key issue for spintronics is the control of the carrier's spin orientation. For conventional half-metals, the spin polarization is fixed at one specific direction, i.e., spin up or spin down. The switch between two spin directions needs the reversion of spontaneous magnetization by external magnetic field, which is not feasible at nanoscale. Thus, the electrical control of carrier's spin polarization is highly desired for spintronics.[12−15]

Since the discovery of graphene, many efforts have been devoted to develop two-dimensional (2D) crystal based spintronics. Graphene has been studied intensively for its gate tunable spin transport,[16] long spin diffusion lengths of about 4 micrometers at room temperature,[17] and unusual electronic properties.[18] However, due to the delocalization character of sp orbitals in carbon materials, significant magnetism and half-metallicity has rarely been observed in experiment. Alternatively, 2D inorganic nanosheets have attracted new attention very recently for their novel electronic and magnetic properties, as well as great potential in electronic and spintronic devices. Experimentally, the 2D graphene-like inorganic nanosheets, such as transition metal dichalcogenides and oxides,[19−21] can be obtained by exfoliating layered crystals. The possible existence of d orbital itinerant magnetism in transition-metal-based 2D nanostructures provides great opportunities to obtain significant half-metallicity and electrical control of spin polarization in these materials.

In this paper, we propose a new 2D $MnPSe_3$ crystal on the basis of first-principles calculations. Bulk $MnPSe_3$ is a layered crystal belonging to the family of $MPX_3$ (M = Mn, Fe, Ni; X = S, Se).[22] The $MnPSe_3$ layers are stacked in an ABC sequence, as shown in Figure 1a. The adjacent $MnPSe_3$ layers are rotated from each other by 60 degree and the vertical interlayer distance (van der Waals gap) is $d_0$ = 3.22 Å. The Se−Se distance between two $MnPSe_3$ layers is about 3.9 Å. Previous experiments have shown that bulk $MnPSe_3$ is an antiferro-

**Received:** May 21, 2014
**Published:** July 18, 2014

   dx.doi.org/10.1021/ja505097m | J. Am. Chem. Soc. 2014, 136, 11065−11069

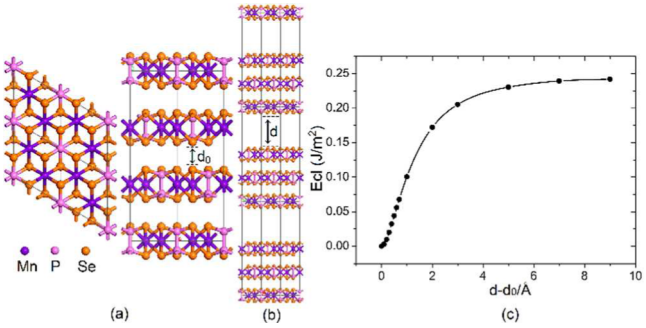


**Figure 1.** (a) Crystal structure of bulk $MnPSe_3$ from top (left part) and side (right part) views. (b) Geometry of introduced fracture used to simulate the exfoliation procedure. (c) Cleavage energy $E_{cl}$ as a function of the separation between two fractured parts.

magnetic semiconductor with an optical energy gap of 2.27 eV[23] and a Néel temperature of 74 K.[24] The lattice dynamics of bulk $MnPSe_3$ was studied in detail by infrared and Raman spectra.[25,26] $MnPSe_3$ can be used as an inelastic electron tunneling barrier[27] and is a potential candidate to realize valley electronics and spintronics.[28]

Here, we find that 2D $MnPSe_3$ can be obtained by exfoliating its bulk with the cleavage energy smaller than that of graphite. The elastic theory analysis indicates that the 2D $MnPSe_3$ possesses relatively high in-plane stiffness to stabilize its free-standing structure. The 2D $MnPSe_3$ crystal is antiferromagnetic (AFM) semiconductor at its ground state. Both electron and hole doping induce its transition from AFM semiconductor to ferromagnetic (FM) half-metal. The Curie temperature is estimated up to 206 K according to Monte Carlo simulations based on the Ising model. In particular, the half-metallic 2D $MnPSe_3$ possesses opposite spin-polarization directions for electron and hole doping which can be controlled by a voltage gate in experiment. These results suggest that 2D $MnPSe_3$ is a potential material to fabricate spintronic devices with electrically controllable spin polarization.

## COMPUTATIONAL PROCEDURES

Our calculations are carried out within the Perdew–Burke–Ernzerhof generalized gradient approximation (GGA)[29] implemented in Vienna ab initio simulation package (VASP).[30] The projector augmented wave (PAW) potential[31] and the plane-wave cutoff energy of 400 eV are used. For bulk $MnPSe_3$, van der Waals interaction (vdW) correction[32,33] is considered. A Monkhorst–Pack k-point mesh of $7 \times 7 \times 3$ is used. For single layer of $MnPSe_3$, a supercell with a vacuum space of 15 Å along the $z$-direction is employed with a k-point mesh of $7 \times 7 \times 1$. Both the lattice constant and the positions of all atoms are relaxed until the force is less than 0.01 eV/Å. The criterion for the total energy is set as $1 \times 10^{-6}$ eV. The optimized lattice constant for bulk $MnPSe_3$ is $a = b = 6.324$ Å and $c = 19.813$ Å, consistent with the experimental value ($a = b = 6.387$ Å, $c = 19.996$ Å).[24] To count the electron correlation effects of Mn 3d orbitals and obtain accurate electronic and magnetic properties of the 2D $MnPSe_3$ crystal, we employ the screened hybrid HSE06 functional,[34,35] which includes the accurate Fock exchange and usually performs much better than the DFT and DFT+U methods.[36−38] The spin–orbital coupling (SOC) correction is not considered here since our test calculations show that it has little influence on our results. Carrier doping is simulated by removing or adding electrons from the system and using a homogeneous background charge to maintain charge neutrality.

## RESULTS AND DISCUSSION

The large van der Waals gap in bulk implies a weak interlayer interaction and the possibility to obtain 2D $MnPSe_3$ crystal with exfoliation method. To verify this guess, we calculate the cleavage energy by introducing a fracture in the bulk (see Figure 1b). The total energy under variation of the separation $d$ between the fractured parts is calculated to simulate the exfoliation procedure.[39] The profile of the cleavage energy vs $d$ values is shown in Figure 1c. It can be seen that the total energy increases with the separation $d$, and gradually converges at the ideal cleavage cohesion energy of about 0.24 J/m$^2$. This value is smaller than the experimentally estimated cleavage energy in graphite (~0.36 J/m$^2$),[40] indicating that the exfoliation of bulk $MnPSe_3$ is feasible in experiment. The theoretical cleavage strength is predicted to be 1.2 GPa by evaluating the maximum derivative of $E_{cl}$ ($d$).[41]

Usually, a high in-plane stiffness is required for the 2D crystal to avoid the curling and obtain free-standing membrane in the exfoliation process. To estimate the in-plane stiffness, the 2D Young's modulus is calculated for the $MnPSe_3$ nanosheet with the following equation,

$$Y_{2D} = A_0\left(\frac{\partial^2 E}{\partial A^2}\right)_{A_0} = \frac{1}{2\sqrt{3}}\left(\frac{\partial^2 E}{\partial a^2}\right)_{a_0} \quad (1)$$

where $E$ is the total energy per unit cell, and $a$ and $A$ are the lattice constant and corresponding surface area, respectively. Figure 2a shows the profile of total energy versus lattice

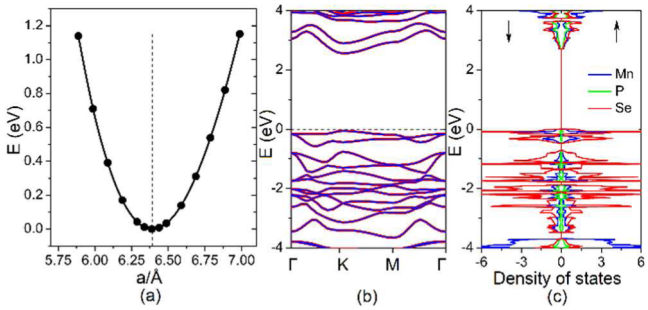


**Figure 2.** (a) Variation of total energy with the lattice constant. (b) Band structure and (c) atom projected density of states for 2D $MnPSe_3$ calculated with HSE06 functional.

constant $a$ for $MnPSe_3$ nanosheet. The calculated $Y_{2D}$ is 36 N/m, which is about 10% of the in-plane stiffness for the ultrastrong material graphene.[42] According to the elastic theory, the gravity induced typical out-of-plane deformation $h$ can be estimated by the formula[42]

$$h/L \approx (\rho g L/Y_{2D})^{1/3} \quad (2)$$

where $\rho = 3.03 \times 10^{-6}$ kg/m$^2$ is the density of 2D $MnPSe_3$, and $L$ is the size of $MnPSe_3$ flakes. For a large $MnPSe_3$ flake with the length $L \approx 100$ $\mu$m, we obtain $h/L \approx 4.4 \times 10^{-4}$, comparable to that of graphene. Therefore, 2D $MnPSe_3$ crystal is able to withstand its own weight and keep free-standing planar structure. Note that the feasibility of cleavage of bulk $MnPSe_3$ has been suggested in previous experiments by successfully intercalating lithium and pyridine into the van der Waals gaps.[43,44] Combined with our evaluated low cleavage energy and strong in-plane stiffness, it is promising that the 2D


dx.doi.org/10.1021/ja505097m | J. Am. Chem. Soc. 2014, 136, 11065−11069

$MnPSe_3$ crystal can be realized by liquid exfoliation techniques.[21]

Magnetic studies show that 2D $MnPSe_3$ crystal prefers AFM coupling, which is more stable than FM state by an energy difference of 55 meV per unit cell. The local magnetic moment of Mn atom is about 4.48 $\mu_B$ where Mn possesses about +2e charge with a high spin state. The calculated electronic band structure indicates that the 2D $MnPSe_3$ crystal is a semiconductor with a direct band gap of 0.94 eV with PBE functional, slightly larger than that of bulk system at the same calculation level (0.85 eV). It is well-known that PBE functional usually underestimates the energy gap and more accurate gap obtained with HSE06 functional is 2.62 eV, as shown in Figure 2b. From the calculated atom projected density of states (PDOS), it can be concluded that the valence bands (VB) near the Fermi level are mainly contributed by Se and Mn atoms, whereas the conduction bands (CB) consist of Se, Mn, and P atom states (Figure 2c).

Next, carrier doping is considered to manipulate the electronic and magnetic properties in 2D $MnPSe_3$ crystal. Previous works have shown that carrier doping can open a big band gap in bilayer graphene that is realized with voltage gate.[45] A carrier-doping induced magnetic transition is also theoretically predicted in phthalocyanine-based organometallic sheet.[46] Figure 3a displays the variation of relative energy of AFM and

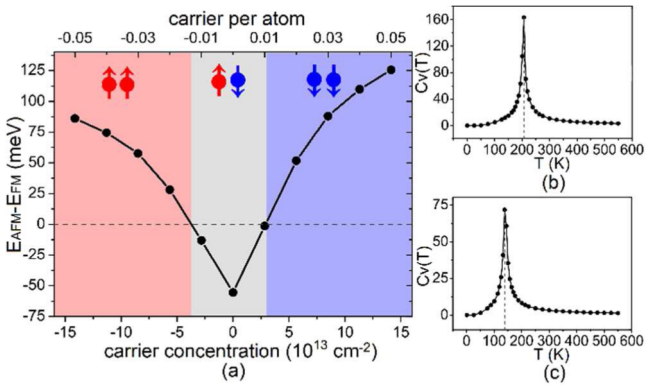


**Figure 3.** (a) Relative energy of AFM and FM states under the variation of carrier concentration for 2D $MnPSe_3$ calculated with HSE06 functional. The positive and negative values are for electron and hole doping, respectively. The up and down arrows indicate up-spin and down-spin, respectively. The simulated specific heat $C_V$ with respect to temperature for (b) electron doping and (c) hole doping with the carrier concentration of $1.4 \times 10^{14}$ cm$^{-2}$.

FM states under carrier doping. Here, we consider the doping concentrations up to $1.4 \times 10^{14}$ cm$^{-2}$ (0.05e charges per atom), which is experimentally accessible. Note that a charge density modulation of $\sim 10^{15}$ cm$^{-2}$ has already been experimentally achieved in many 2D systems by using ionic liquid as gate dielectric, such as gated ZnO and $La_{0.8}Ca_{0.2}MnO$ transistors.[47,48]

With a small amount of electron or hole doping ($<3 \times 10^{13}$ cm$^{-2}$), 2D $MnPSe_3$ retains its antiferromagnetic ground state, while the energy difference between AFM and FM states is rapidly decreased, indicating that the AFM state is greatly destabilized by injected carriers. Further increasing the carrier concentration induces a magnetic transition from AFM to FM state for both electron and hole doping (see Figure 3a). The critical point occurs at about $3 \times 10^{13}$ cm$^{-2}$, which can be easily realized in experiment. Beyond the critical point, 2D $MnPSe_3$ attains net magnetic moment and the FM state becomes the ground state, which can be further enhanced by increasing concentration of the doped carriers. At the concentration of $1.4 \times 10^{14}$ cm$^{-2}$, the FM state is more stable than the AFM state in energy by 126 and 87 meV per unit cell for electron and hole doping, respectively.

For doped 2D $MnPSe_3$ with FM coupling, the Curie temperature $T_c$ is further estimated by using Monte Carlo (MC) simulations with a $42 \times 42 \times 1$ supercell based on the Ising Hamiltonian model,

$$H = -\sum_{i,j} J_{i,j} \mathbf{M}_i \cdot \mathbf{M}_j \tag{3}$$

where $J_{ij}$ is the nearest-neighbor exchange parameter, $\mathbf{M} = 5.0$ $\mu_B$ is the spin magnetic moment per chemical formula. In the simulations, the spins on all magnetic sites flip randomly. Here, we focus on the electron and hole doping with the carrier concentration of $1.4 \times 10^{14}$ cm$^{-2}$, which possesses the largest energy difference between AFM and FM states, thus the highest Curie temperature (Figure 3a). Using the AFM−FM energy difference, the exchange parameter is evaluated to be 0.84 and 0.57 meV for electron and hole doping with the carrier concentration of $1.4 \times 10^{14}$ cm$^{-2}$, respectively. To obtain $T_c$, we calculate the specific heat $C_v = (\langle E^2 \rangle - \langle E^2 \rangle)/T^2$ at first after the system reaches equilibrium at a given temperature. Then $T_c$ is gained by locating the peak position in the $C_v(T)$ plot. From the simulated $C_v(T)$ curve in Figure 3b,c, the Curie temperature is found to be 206 and 138 K for electron and hole doping, respectively. We also calculate the Néel temperature of pristine 2D $MnPSe_3$ to be 88 K. Considering that the interlayer magnetic coupling through the van der Waals gap in bulk $MnPSe_3$ is evaluated to be vanishingly small (about −0.02 meV) and our model only considers the nearest-neighbor exchange interactions, this value (88 K) can be also taken as the Néel temperature of the bulk system, which is in good agreement with the experiment one (74 K), confirming the validity of our model. Note that the calculated Curie temperatures for the carrier doped 2D $MnPSe_3$ significantly exceed the liquid nitrogen temperature.

To study the electronic structure of carrier doped 2D $MnPSe_3$, the band structure and density of states (DOS) are calculated at the doping concentration of $1.4 \times 10^{14}$ cm$^{-2}$. Considering that carrier doping in experiment is usually implemented by a voltage gate and there is an electric field across the sheet, it is necessary to find out the effects of such an electric field on the electronic structure of 2D $MnPSe_3$. Our test calculations show the band structures of 2D $MnPSe_3$ are minimally changed under a rather strong electric field of 1.0 V/Å, indicating the rigidity of band structures of 2D $MnPSe_3$ against external electric fields. Therefore, it is reasonable to neglect the electric field effect during the simulations. From Figure 4, it is clear that both the hole and electron doped 2D $MnPSe_3$ are half-metals, exhibiting 100% spin-polarization around the Fermi level. The spatial charge distribution profiles (Figure 4c,d) of the energy bands across the Fermi level indicate that the half-metallic states are delocalized over the whole structure, ensuring a perfect conducting behavior. The states around the Fermi level are mainly contributed by Se and Mn atoms for the hole-doped 2D $MnPSe_3$, but by all atoms for the electron-doped one (Figure 4e,f).

In particular, the half-metallic 2D $MnPSe_3$ exhibits inverse spin-polarization direction when changing the doping type. As shown in Figure 4, the half-metallicity of hole-doped 2D


dx.doi.org/10.1021/ja505097m | J. Am. Chem. Soc. 2014, 136, 11065−11069

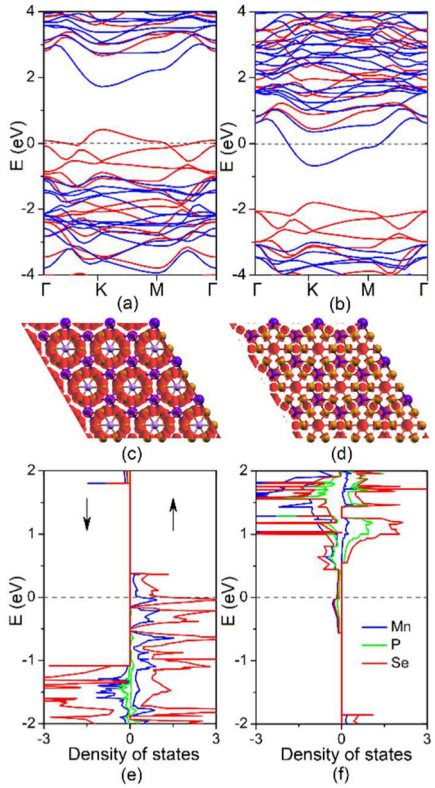


**Figure 4.** Band structure for (a) hole-doped and (b) electron-doped 2D $MnPSe_3$ with the carrier concentration of $1.4 \times 10^{14}$ $cm^{-2}$. (c and d) Corresponding charge distribution of the energy band across the Fermi level plotted with an isovalue of 0.01 e/Å$^3$. (e and f) Atom projected density of states under hole and electron doping, respectively. All the results are calculated with HSE06 functional. Fermi levels are all set to zero.

$MnPSe_3$ presents a complete spin-up polarization, while that for electron-doped one is fully spin-down polarized. This property is actually the same as that of previously proposed bipolar magnetic semiconductors (BMS).[14] Pristine 2D $MnPSe_3$ at FM state is indeed a BMS with the valence band and conduction band possessing opposite spin polarizations, and carrier doping induces a rigid shift of the Fermi level into VB or CB, resulting inverse spin-polarization direction for hole and electron doping. The dependence of spin-polarization direction on the types of doping provides a potential strategy to manipulate the carrier's spin-polarization in 2D $MnPSe_3$ crystal simply by applying a gate voltage. It is well-known that the positive gate voltage extracts electrons from the substance and results in a hole doping effect, whereas the negative gate voltage injects electrons and produces electron doping. Thus, the spin-polarization direction of 2D $MnPSe_3$ crystal can be manipulated by reversing the polarity of the applied gate, making it very attractive for spintronic applications. For example, it is possible to fabricate dual-channel field effect spin-filter and spin-valve, or converter to transform electric signals into spin signals for information transport and storage.[14,15]

## CONCLUSIONS

In summary, we have proposed a new 2D $MnPSe_3$ crystal by exfoliating its bulk. The calculated cleavage energy of bulk $MnPSe_3$ is slightly smaller than that of graphite, indicating the exfoliation of bulk $MnPSe_3$ is possible. Meanwhile, the calculated in-plane stiffness implies that the 2D $MnPSe_3$ crystal can keep its free-standing structure. On the basis of first-principles calculations, we find that 2D $MnPSe_3$ crystal is an AFM semiconductor. Both electron and hole doping induce a magnetic transition from AFM to FM in $MnPSe_3$ nanosheet. The Curie temperature of FM $MnPSe_3$ nanosheet is predicted up to 206 K based on the Ising model MC simulations. In particular, the FM $MnPSe_3$ nanosheet is half-metal with doping-dependent spin-polarization. The carrier's spin-polarization direction is inverse when the doping type changes from electron to hole doping, which can be easily realized by reversing the polarity of the applied gate voltage. These studies first imply that 2D $MnPSe_3$ crystal serves as a potential spintronic material with electric field controlled magnetism.

## AUTHOR INFORMATION

### Corresponding Author

jlyang@ustc.edu.cn

### Notes

The authors declare no competing financial interest.

## ACKNOWLEDGMENTS

This work is partially supported by the National Key Basic Research Program (2011CB921404, 2012CB922001), by NSFC (21121003, 91021004, 20933006, 51172223), by Strategic Priority Research Program of CAS (XDB01020300), by Fundamental Research Funds for the Central Universities (WK2060140014, WK2060190025), by CAS One-Hundred Talent program, and by USTCSCC, SCCAS, Tianjin, and Shanghai Supercomputer Centers.

## REFERENCES

(1) Fert, A. *Rev. Mod. Phys.* **2008**, *80*, 1517−1530.
(2) de Groot, R. A.; Muller, F. M.; Vanengen, P. G.; Buschow, K. H. J. *Phys. Rev. Lett.* **1983**, *50*, 2024−2027.
(3) Li, X.; Wu, X. J.; Yang, J. L. *J. Am. Chem. Soc.* **2014**, *136*, 5664−5669.
(4) Chen, P.; Zhang, G. Y. *Sci. China-Phys. Mech Astron* **2013**, *56*, 207−221.
(5) Kan, E. J.; Li, Z. Y.; Yang, J. L.; Hou, J. G. *J. Am. Chem. Soc.* **2008**, *130*, 4224−4225.
(6) Zhou, J.; Sun, Q. *J. Am. Chem. Soc.* **2011**, *133*, 15113−15119.
(7) Kan, E.; Hu, W.; Xiao, C.; Lu, R.; Deng, K.; Yang, J.; Su, H. *J. Am. Chem. Soc.* **2012**, *134*, 5718−5721.
(8) Du, A.; Sanvito, S.; Smith, S. C. *Phys. Rev. Lett.* **2012**, *108*, 197207.
(9) Abel, M.; Clair, S.; Ourdjini, O.; Mossoyan, M.; Porte, L. *J. Am. Chem. Soc.* **2011**, *133*, 1203−1205.
(10) Bieri, M.; Blankenburg, S.; Kivala, M.; Pignedoli, C. A.; Ruffieux, P.; Müllen, K.; Fasel, R. *Chem. Commun.* **2011**, *47*, 10239−10241.
(11) Lee, J. S.; Wang, X.; Luo, H.; Dai, S. *Adv. Mater.* **2010**, *22*, 1004−1007.
(12) Kato, Y.; Myers, R. C.; Dricoll, D. C.; Gossard, A. C.; Levy, J.; Awschalom, D. D. *Science* **2003**, *299*, 1201−1204.
(13) Nowack, K. C.; Koppens, F. H. L.; Nazarov, Yu. V.; Vandersypen, L. M. K. *Science* **2007**, *318*, 1430−1433.
(14) Li, X. X.; Wu, X. J.; Li, Z. Y.; Yang, J. L.; Hou, J. G. *Nanoscale* **2012**, *4*, 5680−5685.
(15) Li, X. X.; Yang, J. L. *Phys. Chem. Chem. Phys.* **2013**, *15*, 15793−15801.
(16) Cho, S.; Chen, Y. F.; Fuhrer, M. S. *Appl. Phys. Lett.* **2007**, *91*, 123105.
(17) Tombros, N.; Jozsa, C.; Popinciuc, M.; Jonkman, H. T.; van Wees, B. J. *Nature* **2007**, *448*, 571−574.

(18) Novoselov, K. S.; Geim, A. K.; Morozov, S. V.; Jiang, D.; Katsnelson, M. I.; Grigorieva, I. V.; Dubonos, S. V.; Firsov, A. A. *Nature* **2005**, *438*, 197−200.
(19) Coleman, J. N.; Lotya, M.; O'Neill, A.; Bergin, S. D.; King, P. J.; Khan, U.; Young, K.; Gaucher, A.; De, S.; Smith, R. J.; Shvets, I. V.; Arora, S. K.; Stanton, G.; Kim, H. Y.; Lee, K.; Kim, G. T.; Duesberg, G. S.; Hallam, T.; Boland, J. J.; Wang, J. J.; Donegan, J. F.; Grunlan, J. C.; Moriarty, G.; Shmeliov, A.; Nicholls, R. J.; Perkins, J. M.; Grieveson, E. M.; Theuwissen, K.; McComb, D. W.; Nellist, P. D.; Nicolosi, V. *Science* **2011**, *331*, 568−571.
(20) Ataca, C.; Şahin, H.; Ciraci, S. *J. Phys. Chem. C* **2012**, *116*, 8983−8999.
(21) Nicolosi, V.; Chhowalla, M.; Kanatzidis, M. G.; Strano, M. S.; Coleman, J. N. *Science* **2013**, *340*, 1226419.
(22) Le Flem, G. *J. Phys. Chem. Solids* **1982**, *43*, 455−461.
(23) Grasso, V.; Silipigni, L. *J. Opt. Soc. Am. B* **1999**, *16*, 132−136.
(24) Wiedenmann, A.; Mignod, J. R.; Louisy, A.; Brec, R.; Rouxel, J. *Solid State Commun.* **1981**, *40*, 1067−1072.
(25) Bernasconi, M.; Marra, G. L.; Benedek, G.; Miglio, L.; Jouanne, M.; Julien, C.; Scagliotti, M.; Balkanski, M. *Phys. Rev. B* **1988**, *38*, 12089−12099.
(26) Makimura, C.; Sekine, T.; Tanokura, Y.; Kurosaw, K. *J. Phys.: Condens. Mater.* **1993**, *5*, 623−632.
(27) Yamaguchi, K. *Phys. Status Solidi B* **2003**, *236*, 634−639.
(28) Li, X.; Cao, T.; Niu, Q.; Shi, J.; Feng, J. *Proc. Natl. Acad. Sci. U.S.A.* **2013**, *110*, 3738−3742.
(29) Perdew, J. P.; Burke, K.; Ernzerhof, M. *Phys. Rev. Lett.* **1996**, *77*, 3865−3868.
(30) Kresse, G.; Furthmüller, J. *Phys. Rev. B* **1996**, *54*, 11169−11186.
(31) Blöchl, P. E. *Phys. Rev. B* **1994**, *50*, 17953−17979.
(32) Grimme, S. *J. Comput. Chem.* **2006**, *27*, 1787−1799.
(33) Bučko, T.; Hafner, J.; Lebègue, S.; Ángyán, J. G. *J. Phys. Chem. A* **2010**, *114*, 11814−11824.
(34) Heyd, J.; Scuseria, G. E.; Ernzerhof, M. *J. Chem. Phys.* **2003**, *118*, 8207−8215.
(35) Heyd, J.; Scuseria, G. E.; Ernzerhof, M. *J. Chem. Phys.* **2006**, *124*, 219906.
(36) Marsman, M.; Paier, J.; Stroppa, A.; Kresse, G. *J. Phys.: Condens. Mater.* **2008**, *20*, 064201.
(37) Da Silva, J. L. F.; Pirovano, M. V. G.; Sauer, J.; Bayer, V.; Kress, G. *Phys. Rev. B* **2007**, *75*, 045121.
(38) Wen, X.; Martin, R. L.; Roy, L. E.; Scuseria, G. E.; Rudin, S. P.; Batista, E. R.; McCleskey, T. M.; Scott, B. L.; Bauer, E.; Joyce, J. J.; Durakiewicz, T. *J. Chem. Phys.* **2012**, *137*, 154707.
(39) Sachs, B.; Wehling, T. O.; Novoselov, K. S.; Lichtenstein, A. I.; Katsnelson, M. I. *Phys. Rev. B* **2013**, *88*, 201402(R).
(40) Zacharia, R.; Ulbricht, H.; Hertel, T. *Phys. Rev. B* **2004**, *69*, 155406.
(41) Medvedeva, N. I.; Mryasov, O. N.; Gornostyrev, Y. N.; Novikov, D. L.; Freeman, A. J. *Phys. Rev. B* **1996**, *54*, 13506−13514.
(42) Booth, T. J.; Blake, P.; Nair, R. R.; Jiang, D.; Hill, E. W.; Bangert, U.; Bleloch, A.; Gass, M.; Novoselov, K. S.; Katsnelson, M. I.; Geim, A. K. *Nano Lett.* **2008**, *8*, 2442−2446.
(43) Brec, R.; Schleich, D. M.; Ouvrard, G.; Louisy, A.; Rouxel, J. *Inorg. Chem.* **1979**, *18*, 1814−1818.
(44) Otani, S.; Shimada, M.; Kanamaru, F.; Koizumi, M. *Inorg. Chem.* **1980**, *19*, 1249−1251.
(45) Mak, K. F.; Lui, C. H.; Shan, J.; Heinz, T. F. *Phys. Rev. Lett.* **2009**, *102*, 256405.
(46) Zhou, J.; Sun, Q. *Nanoscale* **2014**, *6*, 328−333.
(47) Yuan, H.; Shimotani, H.; Tsukazaki, A.; Ohtomo, A.; Kawasaki, M.; Iwasa, Y. *Adv. Funct. Mater.* **2009**, *19*, 1046−1053.
(48) Dhoot, A. S.; Israel, C.; Moya, X.; Mathur, N. D.; Friend, R. H. *Phys. Rev. Lett.* **2009**, *102*, 136402.